Beam Dynamic Aspects of the TESLA Power Coupler

M. Zhang and Ch. Tang
DESY -MPY- and -MHF-, Notkestrasse 85, 22603 Hamburg, Germany

Abstract

We studied the beam dynamic behavior of the power coupler for the TESLA superconducting cavities. It is found that the transverse kicks due to RF Poynting flow through the coupler is not negligible with respect to the tight beam alignment requirement. It is more than 120 times as strong as the transverse kick factor of a TESLA 9 cell cavity. An estimation of the accumulated transverse kicks by eight such couplers in a TESLA accelerating module is made for various injection phases and initial beam energies. A transverse offset after the first TESLA cryomodule in the TESLA Test Facility (TTF) is estimated to be around 1 to 2 mm. We suggest the use of a symmetrical coupler in conjunction with two back-to-back newly proposed superstructures, which implies a reduction of both transverse kicks and emittance growth and an increase of the overall effective accelerating length of TESLA.

1 INTRODUCTION

TESLA is a superconducting RF based large linear collider project [1]. Its 9 cell superconducting cavity operating at L-band is fed by a coaxial coupler [2]. Due to its non-symmetrical layout, a transverse kick caused by electromagnetic fields is clearly inevitable. The strength of the kicks is proportional to the amount of the power flow. Because of its superconductivity, the cavity itself bears very little ohmic losses. The kick directly scales with the beam power, i.e. the cavity's loaded quality factor Q_l. The electrostatic-like field distribution around the coupler's inner conductor forms a quasi-standing-wave pattern. The field generates a strong kick to a charged beam passing by. Generally speaking, the lower the Q_l, the higher the coupler field, and hence, the bigger the transverse kicks.

In order to address this issue more quantitatively, we conducted an intensive and systematic investigation into the complete dynamic process involving power feeding, bunch injection, kick accumulation, and emittance growth by means of both numerical and analytical methods.

The analytical and numerical results show a good agreement with each other. It is found that the transverse RF kick of the power coupler is more than 120 times as strong as that due to transverse wake fields of a TESLA 9 cell cavity by a 1 mm (σ_z) 1 nC bunch at 1 mm off-axis. The coupler RF kick is always there, even when a bunch is traveling on the ideal trajectory. Since this kick is mainly dependent on Q_l, it is more harmful at lower beam energies. The time dependence of the kicks is directly responsible for the emittance growth, which is found to be as high as 27% for a TESLA accelerating module of eight cavities. The transverse offset at the exit of the first TESLA accelerating module in the TESLA Test Facility (TTF) is found to be $1 \sim 2$ mm with injection energy of 15 MeV and accelerating gradient of 15 MV/m. This number is about 4 times as larger as the TESLA alignment tolerance of 0.5 mm ([1] p100).

Practically, a full field simulation of a superconducting cavity is almost out of the question due to its long filling time. To get round about the obstacle, we first simulated a series of low Q cases and then extrapolated the results to high Q ones. With this technique, we obtained a complete analytical expression for the coupler fields.

Analytical results of the transverse RF kicks agree quite well with the simulations. We found that for different beam directions with respect to the coupler, the kicks are different. It is because of the phase difference between coupler and cavity fields.

With a view to reducing the transverse kicks, we propose to use a symmetrical power coupler. Emittance growth can be, at the same time, reduced by a few percent. With the increased power limit, we can eventually feed two superstructures [3] on both sides of the coupler to further increase the effective accelerating length, on condition that the proposed 4×7 cell setup is feasible for the future TESLA project in terms of RF filling time at $Q_l \sim 10^6$.

In the following sections, we first present the simulation of the dynamic process involving RF switching on, bunch injection, and RF kicking of the beam, from which we construct the analytical expressions for the coupler fields. Then we develop an analytical approach to the estimation of the RF kicks. Next, we give an estimation of transverse offset of a beam due to the accumulated kick effect through a TESLA cryomodule of 8 cavities and 8 couplers. Finally, we present a proposal of using a symmetrical power coupler to drive two superstructures, called "Super^{2}structure".

2 SIMULATION APPROACH

As pointed above, a full field simulation of a superconducting cavity is impossible due to its high Q values. Taking the TESLA cavity as an example, the operating frequency is 1.3 GHz, $Q_l = 10^6$, this means a filling time of $\frac{2Q_l}{\omega} = 245\mu$s. We need some 318,000 RF periods to reach this filling time. As known, for numerical simulations in time domain, one single sine period needs at least four time steps to accomplish. This implies that a total of some 1.3 millions time steps are required for one single RF filling simulation, not to mention particle simulations. It is obviously not practical according to nowadays computer capabilities.

The simulation is done with MAFIA [4] in two steps. The first is to study RF filling process and derive analytical expressions for field components around the coupler, which provide the basis for the analytical approach in Section 3; The second is to compute RF kicks on a beam by the coupler, which serves as a cross-check for the analtyical expressions to be derived in Section 3.

2.1 RF Filling

To determine the complicated field distribution and phase relations along the beam line, we resort to field simulations, since there is no analytical theory available for the near-fields of this particular coupler setup. MAFIA T3 is used to simulate the RF filling process.

2.1.1 Simulation Setup

The geometry used for the simulation is shown in Fig. 1. The two-cell geometry is the minimum to study the establishment of the accelerating mode E01-π. The symmetry plane at y=0 is utilized to further reduce the simulation volume.

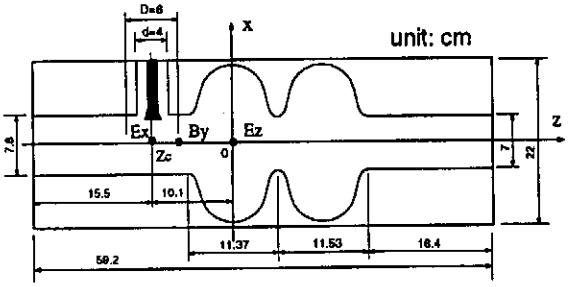

Figure 1: Two-cell geometry used for time-domain simulations. The long drift tubes are determined by the fact that the lowest waveguide mode H11 is to be sufficiently attenuated at both boundaries. Note: λ_{H11} is about 16 cm at f_0=1.3 GHz. The origin is chosen at the center of the first cell. At the three marked points, E_x, B_y, and E_z are measured.

A TEM coaxial wave is applied at the outer terminal at $x = x_{max}$. Two processes take place at RF filling stage. One is the establishment of the mode of interest; The other, taking much longer time, is the filling of the cavity.

The time for a specific mode to settle down depends on the bandwidth of excitation signal and its neighboring modes. The two lowest cavity modes are E01-0 and E01-π (Fig. 2). Because the two eigen-frequencies are quite close to each other ($\Delta f \sim 12$ MHz), a proper selection of the excitation signal is very important. Otherwise, a strong mode beating will occur (Fig. 3), blurring the true relation between field components under study. To avoid the beating, a ramp of 30 carrier's periods is employed. The relative bandwidth can be roughly estimated to be $1/n_p$, with n_p being the number of carrier's periods in the ramp. When the bandwidth is small and the central frequency is close to the eigen-frequency of a certain mode, this particular mode

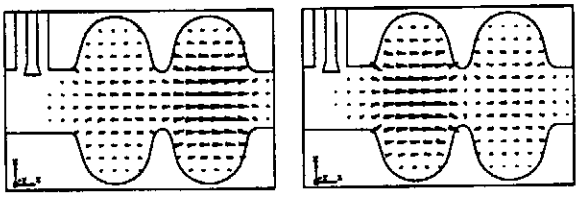

Figure 2: Electric field patterns of the first two E modes: E01-0 (left) and E01-π

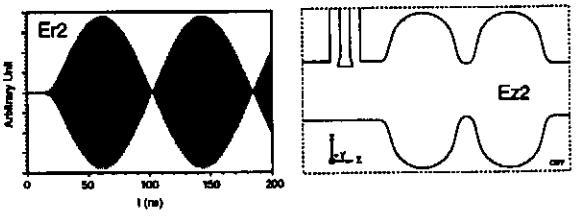

Figure 3: Beating between E01-0 and E01-π modes. The excitation signal at the input port of the coaxial coupler is a sine function with a ramp of 10 RF periods.

can be established in a rather short time. In other words, which mode will be excited largely depends on how close the frequencies of the input signal and the mode are.

It should be pointed out that the setup time of a mode is much shorter than its filling time. Figure 4 shows the E01-π mode setup time is only 74 ns while $Q_l = \infty$.

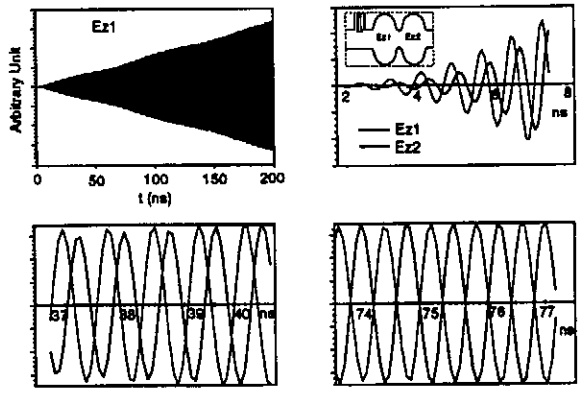

Figure 4: Establishment of mode E01-π. This mode has its electric fields (E_{z1} and E_{z2}) in the two cells with opposite signs. Therefore, whether or not E_{z1} and E_{z2} are exactly 180 degrees out of phase is a sign for the setup of the mode. The last plot shows that the mode is fully established after some 70 ns.

A cavity with $Q_l = \infty$ will never reach its steady state. To shorten the computing time, we introduced a lossy material to lower down Q_l. A series of four Q_l's (1000, 2000, 4000, and 6000) are simulated.

2.1.2 Field Amplitude Ratio

Near the coupler, three field components are of great interest. They are E_x, B_y, and E_z. In this paper, E_x is measured on axis right below the coupler's inner conductor; B_y

on axis and 3 cm to the right of E_x; E_z on axis at the center of the cell close to the coupler (Fig. 1).

The RF filling process for Q_l=6000 is presented in Fig. 5. Table 1 lists $\hat{E}_x$, $c\hat{B}_y$, and $\hat{E}_z$ after the cavity is saturated.

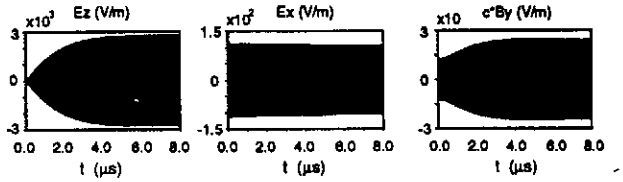

Figure 5: Amplitude development of E_x, B_y, and E_z of mode E01-π at Q_l=6000. The RF filling process can be clearly seen.

Q_l	$\hat{E}_x$ (V/m)	$c\hat{B}_y$ (V/m)	$\hat{E}_z$ (V/m)
1000	110	13.5	400
2000	110	15.0	800
4000	110	16.5	1600
6100	110	24.0	2700

Table 1: Amplitudes of E_x, cB_y, and E_z after filling time

Based on Table 1, we are able to derive the following relations:

$$\alpha_E \equiv \frac{\hat{E}_x}{\hat{E}_z} \approx \frac{10^3}{4Q_l}, \tag{1}$$

$$\alpha_B \equiv \frac{c\hat{B}_y}{\hat{E}_x} \approx 0.075(2 + 10^{-4}Q_l). \tag{2}$$

Hat "$\hat{E}$" denotes peak values. With the above relations, we can obtain coupler fields at any specific Q_l by extrapolation, thanks to the linear scaling law.

2.1.3 Spatial and Temporal Dependence

The spatial field distributions along the beam axis are shown in Fig. 6. As an approximation, we use following functions for the spatial dependence of E_x and B_y near the coupler,

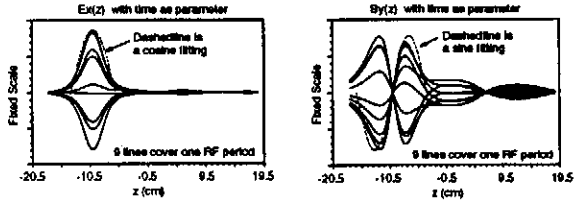

Figure 6: Spatial dependence of E_x and B_y. On the left-hand side of the coupler, B_y is a pure standing wave. Each plot has 9 solid curves showing the respective components at 9 different time snapshots, which cover one RF period. The dotted lines are cosine and sine fittings.

$$E_x(z) = \begin{cases} \hat{E}_x \cos\frac{\pi}{D}(z - z_c) & |z - z_c| \le \frac{D}{2} \\ 0 & \text{otherwise} \end{cases} \tag{3}$$

and

$$B_y(z) = \begin{cases} \hat{B}_y \sin\frac{\pi}{D}(z - z_c) & |z - z_c| \le D \\ 0 & \text{otherwise,} \end{cases} \tag{4}$$

where z_c is the coupler coordinate, $D \equiv \frac{3d}{2}$ and d is the outer diameter of the coupler (see Fig. 1).

Figure 7 shows E_x and B_y phases at different points along the axis for different Q_l's. The traveling wave characteristic of E_x and B_y between the coupler and the first cell can be clearly seen and they gradually tend to standing waves with the increase of Q_l. E_x is $-\frac{\pi}{2}$ and B_y π out of phase with respect to E_z for $Q_l \to 0$, while for $Q_l \to \infty$, they are $-\pi$ and $\frac{\pi}{2}$, respectively.

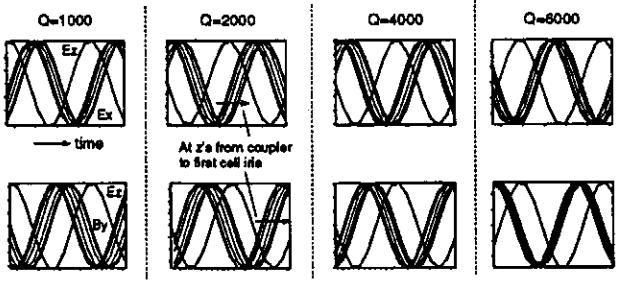

Figure 7: Temporal dependence of E_x and B_y. The reference is E_z, which we know as bunch injection phase. In each plot, a bunch of 8 curves are shown, which are monitored at a series of 8 points on axis: z=-9.5 cm, -8.5 cm, $\cdots$, -3.5 cm, -2.5 cm, from left to right, respectively. The top row is E_x while the bottom B_y. With the increase of Q_l, the phase widths for both field components are getting narrower and narrower and they tend to their corresponding phases at the cell center (z=0). The broader the phase width, the faster the electromagnetic energy flows.

To facilitate the analyses below, we only use the two extreme phase values for $Q_l \to 0$ (low Q phases) and $Q_l \to \infty$ (high Q phases) and denote them by

$$\text{for low Qs} \quad \phi_{E,l} = -\frac{\pi}{2} \quad \text{and} \quad \phi_{B,l} = \pi, \tag{5}$$

$$\text{for high Qs} \quad \phi_{E,h} = -\pi \quad \text{and} \quad \phi_{B,h} = \frac{\pi}{2}. \tag{6}$$

A complete set of expressions for E_x and B_y near the coupler can be written as follows:

$$E_x(z,t) = \hat{E}_x \cos\frac{\pi}{D}(z - z_c)\cos(\omega t + \phi_0 + \phi_E)$$

$$|z - z_c| \le \frac{D}{2} \tag{7}$$

and

$$B_y(z,t) = \hat{B}_y \sin\frac{\pi}{D}(z - z_c)\cos(\omega t + \phi_0 + \phi_B)$$

$$|z - z_c| \le D, \tag{8}$$

where ϕ_0 is injection phase, i.e. the RF phase at $t = 0 \cap z = 0$, ϕ_E and ϕ_B are to be substituted with $\phi_{E,l}$ and $\phi_{B,l}$ for low Q cases or with $\phi_{E,h}$ and $\phi_{B,h}$ for high Q ones. $\hat{E}_x$ and $\hat{B}_y$ are given by Eqs. 1 and 2, as long as the peak accelerating gradient $\hat{E}_z$ is specified.

For example, given $Q_l = 10^6$, $\hat{E}_z = 30$ MV/m, then $\alpha_E = \frac{\hat{E}_x}{\hat{E}_z} = 1/4000$ and $\alpha_B = \frac{c\hat{B}_y}{\hat{E}_x} = 7.7$, so we obtain: $\hat{E}_x = 7.5$ kV/m and $c\hat{B}_y = 57.8$ kV/m.

It is instructive to know that the E_x and B_y phase relations at initial stage of RF filling are different from those at steady state. The traveling waves of E_x and B_y form a real Poynting power flow in $+z$ direction. At initial filling stage, this flow is stronger than that at steady state, for the cavity itself stores energy. To illustrate the phase development during the filling time, we also present B_y phase for Q_l=6000 at initial stage together with that at final stage in Fig. 8. The widened phase spread means a faster en-

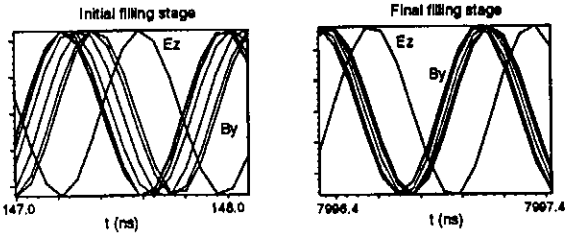

Figure 8: B_y phase width at initial and final RF filling stages

ergy flow. This phenomenon indicates that at initial filling stage, the Poynting flow behaves as if the cavity had a lower Q value. This statement can be easily justified by studying Fig. 7, where the phase spread becomes narrower and narrower with the increase of Q values, converging to the corresponding phases in the cell. A qualitative illustration of the phase and wave distributions along axis is presented in Fig. 9.

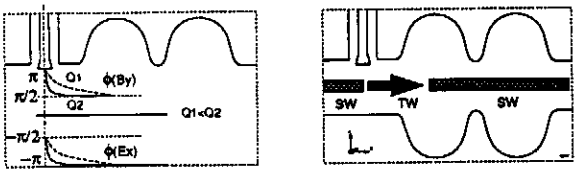

Figure 9: E_x and B_y phase and wave distributions. "SW" stands for standing wave and "TW" for traveling wave.

2.2 *Coupler Kicks*

The kick simulation is performed with the self-consistent code TS3 of MAFIA. In order to reduce the mesh size, we use only one cell here. Full 3D geometry is used (Fig. 10), taking no y=0 symmetry for the sake of a more stable particle trajectory. The cavity has $Q_l = 6000$. RF power is fed through the coaxial coupler at t=0. A 1 nC 5MeV bunch of length 20 ps is injected at t=100 ns from either side of

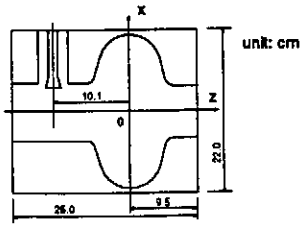

Figure 10: One-cell geometry used for particle simulations

the cavity with $\phi_0 = -45.6°$ off-crest of the accelerating E_z field at the center of the cell. As known, the mode setup time is very short, only a few tens of RF periods. The bunch is injected at the initial stage of the filling process which justifies the use of the low Q phase relation. Some general simulation data are listed in Table 2.

Total number of mesh points	191,000
Minimum mesh steps x/y/z	2 mm
Geometry	x=(-11,11) cm y=(-11,11) cm z=(-15.5,9.5) cm
Integration time step	3.66 ps
Total number of time steps	59,000
CPU time	11 hours (SUN Sparc2)

Table 2: Computational settings for the kick simulation

Both beam directions are studied. The results are presented in Fig. 11. The kick divergence for both directions is

$$x'_{+z,num} = 2.9 \times 10^{-4} \text{ and } x'_{-z,num} = 5.8 \times 10^{-4}. \quad (9)$$

3 ANALYTICAL FORMULATION

In the following, we will derive single particle dynamics through the coupler RF fields. Let us start with the Lorentz force

$$\vec{F}(z,t) = q[\vec{E}(z,t) + \vec{v} \times \vec{B}(z,t)], \quad (10)$$

$$t = \frac{z}{|\vec{v}|}\vec{a_v} \cdot \vec{a_z} \equiv \frac{z}{|\vec{v}|}s \quad (\vec{v} \equiv |\vec{v}|\vec{a_v})$$

$$\text{with } s \equiv \frac{1}{s} \equiv \vec{a_v} \cdot \vec{a_z}. \quad (11)$$

$$dt = \frac{dz}{|\vec{v}|}s \quad (12)$$

$$\begin{aligned} \vec{P} &= \int_{t_1}^{t_2} \vec{F} dt = \int_{z_1}^{z_2} \vec{F}(z, \frac{z}{|\vec{v}|}s)\frac{dz}{|\vec{v}|}s \\ &= q\int_{z_1}^{z_2} [\vec{E}(z, \frac{z}{|\vec{v}|}s) + |\vec{v}|\vec{a_v} \times \vec{B}(z, \frac{z}{|\vec{v}|}s)]\frac{dz}{|\vec{v}|}s \end{aligned} \quad (13)$$

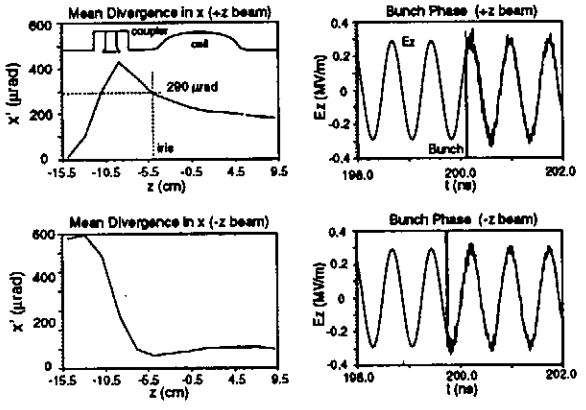

Figure 11: Kick simulation results. The top row is for +z beam direction while the bottom for -z. In this particular RF setting, the -z beam direction seems more harmful. Since this case is only used for checking the analytical expressions in the next section, it doesn't necessarily imply that the -z direction is just worse in reality. The righthand side column shows the bunch phase, from which we know it is -45.6 degree off-crest.

For $\vec{E} = E_x\vec{a_x}$, $\vec{B} = B_y\vec{a_y}$, and $\vec{v} = c\vec{a_z}$, the above equation is simplified to

$$P_x = q\int_{z_1}^{z_2}[E_x(z,\frac{z}{c}) - cB_y(z,\frac{z}{c})]\frac{dz}{c}. \quad (14)$$

It is clear that for beam direction in $-z$, just replace all c by $-c$. By inserting Eqs. 7 and 8 into Eq. 14, we get

$$P_x = \underbrace{\frac{q}{c}\int_{z_1}^{z_2} E_x(z,\frac{z}{c})dz}_{\equiv P_{x,E}} \underbrace{-\frac{q}{c}\int_{z_1}^{z_2} cB_y(z,\frac{z}{c})dz}_{\equiv P_{x,B}}, \quad (15)$$

with

$$P_{x,E} = \frac{q}{c}\int_{z_c-\frac{D}{2}s}^{z_c+\frac{D}{2}s} \hat{E}_x \cos\frac{\pi}{D}(z-z_c)\cos(\frac{\omega}{c}z+\phi_0+\phi_E)dz \quad (16)$$

and

$$P_{x,B} = \frac{q}{c}\int_{z_c-Ds}^{z_c+Ds} c\hat{B}_y \sin\frac{\pi}{D}(z_c-z)\cos(\frac{\omega}{c}z+\phi_0+\phi_B)dz \quad (17)$$

where $s = -1$ for $-c$. After some manipulations, we obtain

$$P_{x,E} = \frac{q\hat{E}_x}{|c|}\frac{\frac{2\pi}{D}}{(\frac{\pi}{D})^2-(\frac{\omega}{c})^2}\cos(\frac{\omega D}{2c})\cos(\frac{\omega}{c}z_c+\phi_0+\phi_E) \quad (18)$$

and

$$P_{x,B} = \frac{qc\hat{B}_y}{|c|}\frac{\frac{2\pi}{D}}{(\frac{\pi}{D})^2-(\frac{\omega}{c})^2}\sin(\frac{\omega D}{c})\sin(\frac{\omega}{c}z_c+\phi_0+\phi_B). \quad (19)$$

Substituting $\frac{\omega}{c} = \frac{2\pi}{\lambda}$ and $D = \frac{3d}{2}$, it yields

$$\begin{aligned} P_x &= P_{x,E} + P_{x,B} \\ &= \frac{q}{|c|}\frac{\frac{3d}{\pi}}{1-(\frac{3d}{\lambda})^2} \\ &\quad \left[\hat{E}_x\cos(\pi\frac{3d}{2\lambda})\cos(2\pi\frac{z_c}{\lambda}+\phi_0+\phi_E)+\right. \\ &\quad \left. c\hat{B}_y\sin(\pi\frac{3d}{\lambda})\sin(2\pi\frac{z_c}{\lambda}+\phi_0+\phi_B)\right] \\ &= \frac{q\alpha_E\hat{E}_z d}{|c|}\frac{\frac{3}{\pi}}{1-(\frac{3d}{\lambda})^2} \\ &\quad \left[\cos(\pi\frac{3d}{2\lambda})\cos(2\pi\frac{z_c}{\lambda}+\phi_0+\phi_E)+\right. \\ &\quad \left. s\alpha_B\sin(\pi\frac{3d}{\lambda})\sin(2\pi\frac{z_c}{\lambda}+\phi_0+\phi_B)\right]. \quad (20) \end{aligned}$$

Note: c was substituted by λ. So for $-z$ beam direction, change all λ to $-\lambda$ and s to -1.

For low Q_l, $\phi_E = \phi_{E,l} = -\frac{\pi}{2}$, $\phi_B = \phi_{B,l} = \pi$,

$$\begin{aligned} P_x &= \frac{q\alpha_E\hat{E}_z d}{|c|}\frac{\frac{3}{\pi}}{1-(\frac{3d}{\lambda})^2}\left[\cos(\pi\frac{3d}{2\lambda})-\right. \\ &\quad \left. s\alpha_B\sin(\pi\frac{3d}{\lambda})\right]\sin(2\pi\frac{z_c}{\lambda}+\phi_0), \quad (21) \end{aligned}$$

and for high Q_l, $\phi_E = \phi_{E,h} = -\pi$, $\phi_B = \phi_{B,h} = \frac{\pi}{2}$,

$$\begin{aligned} P_x &= \frac{q\alpha_E\hat{E}_z d}{|c|}\frac{\frac{3}{\pi}}{1-(\frac{3d}{\lambda})^2}\left[-\cos(\pi\frac{3d}{2\lambda})+\right. \\ &\quad \left. s\alpha_B\sin(\pi\frac{3d}{\lambda})\right]\cos(2\pi\frac{z_c}{\lambda}+\phi_0). \quad (22) \end{aligned}$$

Note: ϕ_0 is dependent on the beam direction. If it is ϕ_0 for a $+z$ beam, then it is $\pi+\phi_0$ for the $-z$ beam, since we need an acceleration of beam for both directions.

By inserting the parameters used in Section 2.2 into Eq. 21, i.e. $\hat{E}_x = 1.12\times10^5, \alpha_B = \frac{c\hat{B}_y}{\hat{E}_x} = 0.112$, we get

$$x'_{+z,ana} = 2.64\times10^{-4} \text{ and } x'_{-z,ana} = 6.07\times10^{-4}. \quad (23)$$

By comparing the above results with the numerical ones (Eq. 9), we find they agree within 10%. Note: we have used the low Q formula. This nice agreement provides a solid basis for an extrapolation to high Q cases. It is worth to know that the RF kick amplitude and the direction are independent of particle types. That is, either electron or positron will experience the identical kick (value and direction), as long as they are both to be accelerated or decelerated.

Let us estimate how big the kick P_x is for the actual TESLA cavity settings. Given $Q_l = 5\times10^6, \hat{E}_z = 30$ MV/m, $\phi_0 = -15^o, d = 4$ cm, $\lambda = 23$ cm, $z_c = -10.1$

cm, we get

$$P_x = 2.9 \times \cos(2\pi\frac{z_c}{\lambda} + \phi_0) \quad \text{(keV/c)} \qquad (24)$$
$$= 2.9 \times \cos(2\pi\frac{-10.1}{-23} + \pi - \phi_0) = 2.3 \quad \text{(keV/c)}.$$

Note: The negative λ and the additional π are both due to -z beam direction. We have used the high Q formula here. The kick is towards the coupler. For other ϕ_0's and Q_l's in -z, see Fig. 12, where the high Q formula is used (Eq. 22).

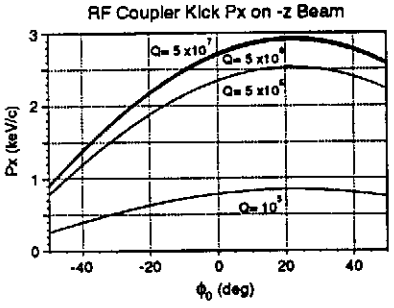

Figure 12: Transverse kick versus bunch injection phase for the TTF operation settings. It is worth to point out that below a certain Q_l value, the kick drops dramatically down to zero and then goes to the opposite sign. This Q_l value is probably only dependent on coupler geometry and RF phase. It implies that the electric and magnetic kicks cancel each other. We need to study this phenomenon more closely.

To give a quantitative reference, we make a comparison of the RF kick with the transverse kick factor (k_t^{9cell}) due to wake fields in a 9 cell TESLA cavity. We know that for a 1mm (σ_z) 1 nC bunch, k_t^{9cell} is equal to 18 V/nC/mm [5]. The RF kick of the coupler $P_x = 2.3$ keV/c, which is independent of bunch charge and loosely of axis offset, is equivalent to a wake field kick experienced by a 1 mm (σ_z) 1 nC bunch traversing through a 9 cell TESLA cavity with an offset of 120 mm from the axis, or it is more than **120** times stronger than the wake field kick at 1 mm offset (1 mm σ_z and 1 nC). Another equivalence can be made to the wake field kick (k_t^{cplr}) of the coupler itself. Simulation shows $k_t^{cplr} = \frac{k_t^{9cell}}{5.3}$ for a 1 mm σ_z bunch, i.e. $k_t^{cplr} = 3.4$ V/nC (on-axis). To reach the 2.3 keV/c RF kick, the bunch charge should be as high as 676 nC!

From Eqs. 21 and 22, it is clear that the RF kicks are different along a bunch length, increasing the bunch's uncorrelated divergence $\sigma_{\Delta P_x}$, hence the bunch's normalized emittance $\epsilon_{n,x}$. The relative increase of emittance can be estimated with

$$\frac{d\epsilon_{n,x}}{\epsilon_{n,x}} = (1+\alpha^2)\left(\frac{d\sigma_x}{\sigma_x} + \frac{d\sigma_{P_x}}{\sigma_{P_x}} - \frac{d\sigma_{xP_x}}{\sigma_{xP_x}}\right) + \frac{d\sigma_{xP_x}}{\sigma_{xP_x}}. \qquad (25)$$

It can be derived as follows. Start with the normalized emittance in x

$$\epsilon_{n,x}^2 = \sigma_x^2\sigma_{P_x}^2 - \sigma_{xP_x}^2, \qquad (26)$$

where

$$\sigma_x^2 = \frac{1}{N}\sum_i (x_i - \bar{x})^2$$
$$\sigma_{P_x}^2 = \frac{1}{N}\sum_i (P_{x,i} - \bar{P}_x)^2$$
$$\sigma_{xP_x} = \frac{1}{N}\sum_i (x_i - \bar{x})(P_{x,i} - \bar{P}_x),$$

we have

$$\begin{aligned}\epsilon_{n,x}d\epsilon_{n,x} &= \sigma_{P_x}^2\sigma_x\,d\sigma_x + \sigma_x^2\sigma_{P_x}\,d\sigma_{P_x} - \sigma_{xP_x}\,d\sigma_{xP_x} \\ &= (\sigma_x\sigma_{P_x})^2\left(\frac{d\sigma_x}{\sigma_x} + \frac{d\sigma_{P_x}}{\sigma_{P_x}}\right) - \sigma_{xP_x}^2\frac{d\sigma_{xP_x}}{\sigma_{xP_x}} \\ &= (\sigma_x\sigma_{P_x})^2\left(\frac{d\sigma_x}{\sigma_x} + \frac{d\sigma_{P_x}}{\sigma_{P_x}} - \frac{d\sigma_{xP_x}}{\sigma_{xP_x}}\right) + \\ &\quad \epsilon_{n,x}^2\frac{d\sigma_{xP_x}}{\sigma_{xP_x}}, \qquad (27)\end{aligned}$$

and then

$$\frac{d\epsilon_{n,x}}{\epsilon_{n,x}} = \frac{(\sigma_x\sigma_{P_x})^2}{\epsilon_{n,x}^2}\left(\frac{d\sigma_x}{\sigma_x} + \frac{d\sigma_{P_x}}{\sigma_{P_x}} - \frac{d\sigma_{xP_x}}{\sigma_{xP_x}}\right) + \frac{d\sigma_{xP_x}}{\sigma_{xP_x}}. \qquad (28)$$

Since

$$\frac{(\sigma_x\sigma_{P_x})^2}{\epsilon_{n,x}^2} = \beta\gamma = 1 + \alpha^2,$$

so Eq.25 gets proved.

Assume that the coupler kick is instantaneous, then $d\sigma_x = 0$. If the bunch comes into the coupler fields with $\alpha = 0$, Eq.25 can be further simplified to

$$\frac{d\epsilon_{n,x}}{\epsilon_{n,x}} = \frac{d\sigma_{P_x}}{\sigma_{P_x}}. \qquad (29)$$

$$d\sigma_{P_x} = \frac{dP_x}{d\phi_0}\sigma_z, \qquad (30)$$

where σ_z is bunch length. With Eq. 24, we get

$$\frac{dP_x}{d\phi_0} = -2.9 \times \sin(2\pi\frac{z_c}{\lambda} + \phi_0) = 1.74 \ \text{(keV/c)}. \qquad (31)$$

At the entrance of the first cryomodule, the bunch length is σ_z =1 mm = 1.56° = 0.027 radian, so $d\sigma_{P_x} = 47$ eV/c, i.e. $d\sigma_{(\gamma\beta_x)} = 9.2 \times 10^{-5}$. Assume that the bunch emittance in the first cryomodule is constant and equal to $\epsilon_{n,x} = 0.6\pi$ mm-mrad and an average $\sigma_x = 0.2$ mm (TTF FEL 0.5 nC optimized case [6]), since we have assumed $\alpha = 0$, then we can easily obtain $\sigma_{(\gamma\beta_x)} = 3 \times 10^{-3}$. And finally, we get

$$\frac{d\epsilon_{n,x}}{\epsilon_{n,x}} = \frac{d\sigma_{P_x}}{\sigma_{P_x}} = \frac{d\sigma_{(\gamma\beta_x)}}{\sigma_{(\gamma\beta_x)}} = \frac{9.2 \times 10^{-5}}{3 \times 10^{-3}} \approx 3\%. \qquad (32)$$

For an entire cryomodule with eight couplers, there will be as high as 27% emittance growth. For the FEL operation, this number is already too large to tolerate.

4 ESTIMATION OF OVERALL RF KICK THROUGH THE FIRST CRYOMODULE OF TTF

The TESLA accelerating module (cryomodule) is composed of eight 9 cell cavities, each of which has an RF power coupler. The couplers are mounted at the downstream end of the cavities. The gap between two cavities is $\frac{3\lambda}{2}$, i.e. 3 cells length. The setup is shown in Fig. 13.

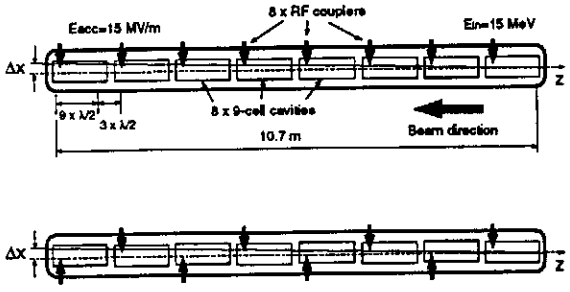

Figure 13: Top: The original TESLA accelerating module; Bottom: Alternating RF coupler placement – A proposal to reduce RF coupler kicks.

To make a quick and accurate estimation, we traced a single particle through the structure with a lumped transverse kick from the RF couplers. The accumulated offset Δx as function of initial energy E_0, injection phase ϕ_0, accelerating gradient E_{acc}, Q_l, and initial offset x_0 is presented in Fig. 14, where the base settings are E_0=15 MeV, $\phi_0 = -15°$, E_{acc}=15 MV/m, $Q_l = 10^6$, and x_0=0. It is

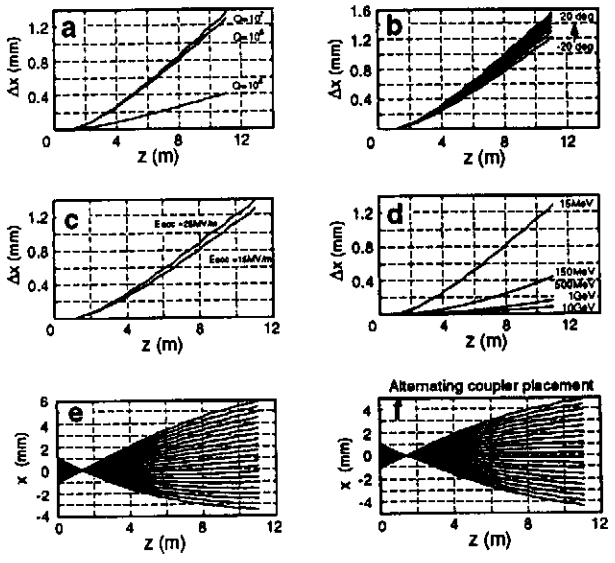

Figure 14: Accumulated offset due to kicks from the RF couplers in the first cryomodule of TTF linac. The initial bunch offset in x is zero for plots **a** to **d**, while plots **e** and **f** show the initial offset dependence. Plot **f** is with an alternating RF coupler placement, which shows a reduction of the accumulated offset by a factor of 5.3.

seen that for the current TTF operating parameters, the first cryomodule will kick the beam centroid 1 ~ 2 mm away from the cavity axis. The value has a strong dependence on various parameters like ϕ_0 and beam loading. Since the absolute value of the RF kick is independent of initial beam energy, it is then especially harmful for low energy beam. More importantly, emittance growth at lower energies, say, in the capture cavity and the first cryomodule, becomes untolerable for the TTF FEL operation. All these will be checked by a dedicated measurement on TTF [7].

5 SYMMETRICAL RF POWER COUPLER AND SUPER^{2}STRUCTURE

It is seen that the strong RF kick comes from the one-sided static pattern of the electric and magnetic fields in the neighborhood of the coupler. A natural solution is to use a symmetrical coupler (Fig. 15). We simulated such a

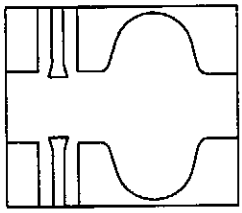

Figure 15: A possible layout of a symmetrical RF coupler, composed of two coaxial couplers sitting opposite to each other across the beam line.

symmetrical coupler with the identical beam and RF settings as used in the previous simulations. It is found that the RF kick can be reduced dramatically, ideally being zero if on axis. With particle simulations, emittance growth is found to be reduced by some 17%. We propose to use such symmetrical coupler to feed two superstructures connected back-to-back in the middle to further exploit the effective accelerating length of the entire linac and to fully utilize the power capability of the symmetrical coupler (Fig. 16). We

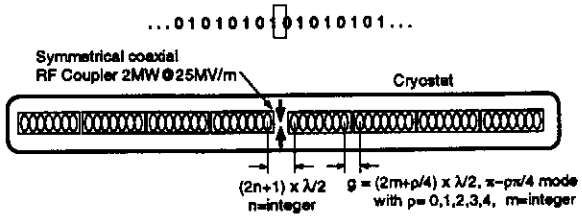

Figure 16: Super^{2}structure proposal for the TESLA Collider. The symmetrical coupler ought to provide a 2 MW RF power, 1 MW [8] for each 4 cavities at 10 mA beam current. The total energy gain is 156 MeV with E_{acc}=25 MV/m. Mode "a-b" is defined as (cell-to-cell)-(cavity-to-cavity) phase advance.

refer to this setup as super^{2}structure. There are two main advantages of this setup over the original TESLA one. The RF kick due to the unsymmetrical field pattern is reduced substantially. And if any, the upstream and downstream

kicks will cancel each other, since they are opposite in sign; The effective accelerating length of a super^{2}structure is 13% higher according to the following simple geometrical calculation, taking n=1, ρ=0, and m=1. It makes this option more attractive than the alternating coupler scheme (Fig. 14). The net geometrical length in unit of cells in one super^{2}structure cryomodule is 8x8=64 cells; Accelerating length is 8x7=56 cells. For the original TESLA module, they are 8x12-3=93 cells and 8x9=72 cells, respectively. The gain ratio is then

$$\frac{\text{super}^2\text{structure } \frac{56}{64}}{\text{original TESLA } \frac{72}{93}} = 1.13. \qquad (33)$$

6 CONCLUSIONS

We made a systematic investigation of the transverse kick exerted on beams by the TESLA power coupler. The analytical and numerical results agree quite well with each other. They showed that the effect is not negligible, especially at lower energies. With the current TTF operation parameters, the accumulated kick by the first TTF cryomodule will deflect the beam $1 \sim 2$ mm from the ideal axis. The kick has a strong dependence on beam loading. Emittance growth is found to be as high as 27% in the first cryomodule.

We proposed to use a symmetrical coupler to drive two superstructure in the middle, which not only further exploits the effective accelerating length of TESLA but also dramatically reduces the RF kicks. The superstructure concept reduces the total number of power couplers by a factor of 4, while the symmetrical coupler scheme doubles the number. So the net reduction of number of couplers is still a factor of 2. Another advantage of the back-to-back superstructure layout lies in that the RF kicks for upstream and downstream directions cancel each other, further reducing the RF kicks on an off-axis beam by the symmetrical couplers.

7 REFERENCES

[1] R. Brinkmann, G. Materlik, J. Rossbach, A. Wagner (eds.), *Conceptual Design of a 500 GeV e+e- Linear Collider with Integrated X-ray Laser Facility*, DESY 1997-048 and ECFA 1997-182

[2] D. Proch, P. Schmüser (eds.), *TESLA Input Coupler Workshop*, DESY Print, TESLA Report 96-09, August 1996

[3] J. Sekutowicz, M. Ferrario, Ch. Tang, *Superconducting Superstructure for TESLA Collider*, DESY Print, TESLA Report 98-08, April 1998

[4] MAFIA version 4.013, CST GmbH, http://www.cst.de, Lauteschlägerstraße 38, D-64289 Darmstadt, Germany

[5] A. Mosnier, *Longitudinal and Transverse Wakes for the TESLA Cavity*, DESY Print, TESLA Report 93-11, May 1993

[6] M. Zhang, T. Limberg, PARMELA and COMFORT optimization results

[7] S. Fartoukh, *RF Steering Experiments on TTF*, DESY Print, TESLA Report 98-01, February 1998

[8] D. Proch, *TESLA collaboration meeting*, March 1998